Available online at www.sciencedirect.com
SCIENCE DIRECT®
Planetary and Space Science 53 (2005) 498–507
Planetary and Space Science
www.elsevier.com/locate/pss

Jupiter's ammonia clouds—localized or ubiquitous?

S.K. Atreya[a,*], A.S. Wong[a], K.H. Baines[b], M.H. Wong[c], T.C. Owen[d]

[a]*Department of Atmospheric, Oceanic, and Space Sciences, The University of Michigan, Ann Arbor, MI 48109-2143, USA*
[b]*Jet Propulsion Laboratory, California Institute of Technology, Pasadena, CA 91109, USA*
[c]*Astronomy Department, University of California, Berkeley, CA 94720, USA*
[d]*Institute for Astronomy, University of Hawaii, Honolulu, HI 96822, USA*

Received 10 November 2003; received in revised form 9 April 2004; accepted 13 April 2004
Available online 8 February 2005

Abstract

From an analysis of the Galileo Near Infrared Imaging Spectrometer (NIMS) data, Baines et al. (Icarus 159 (2002) 74) have reported that spectrally identifiable ammonia clouds (SIACs) cover less than 1% of Jupiter. Localized ammonia clouds have been identified also in the Cassini Composite Infrared Spectrometer (CIRS) observations (Planet. Space Sci. 52 (2004a) 385). Yet, ground-based, satellite and spacecraft observations show that clouds exist everywhere on Jupiter. Thermochemical models also predict that Jupiter must be covered with clouds, with the top layer made up of ammonia ice. For a solar composition atmosphere, models predict the *base* of the ammonia clouds to be at 720 mb, at 1000 mb if N/H were $4\times$ solar, and at 0.5 bar for depleted ammonia of $10^{-2}\times$ solar (Planet. Space Sci. 47 (1999) 1243). Thus, the above NIMS and CIRS findings are seemingly at odds with other observations and cloud physics models. We suggest that the clouds of ammonia ice are ubiquitous on Jupiter, but that spectral identification of all but the freshest of the ammonia clouds and high altitude ammonia haze is inhibited by a combination of (i) dusting, starting with hydrocarbon haze particles falling from Jupiter's stratosphere and combining with an even much larger source—the hydrazine haze; (ii) cloud properties, including ammonia aerosol particle size effects. In this paper, we investigate the role of photochemical haze and find that a substantial amount of haze material can deposit on the upper cloud layer of Jupiter, possibly enough to mask its spectral signature. The stratospheric haze particles result from condensation of polycyclic aromatic hydrocarbons (PAHs), whereas hydrazine ice is formed from ammonia photochemistry. We anticipate similar conditions to prevail on Saturn.

1. Introduction

Jupiter is covered with clouds. However, identification of the composition of these clouds has eluded planetary scientists. Thermochemical models imply that the uppermost visible clouds of Jupiter are all composed of ammonia ice. Ground-based observations cannot detect even the strong ammonia ice signatures (ν_2 and ν_3 bands at 10 and 3 μm, respectively) due to ozone absorption at 10 μm and the H_2O and CO_2 absorptions in the 3 μm region in the earth's atmosphere. Observations from the Infrared Space Observatory (ISO) in the 2.7–3 μm range first positively indicated the presence of spectrally identifiable ammonia clouds on Jupiter (Brooke et al., 1998). This landmark result indicated that the signature was produced by relatively large particles, approximately 10 μm in radius. However, the ISO data provided little information on the actual spatial distribution of the spectrally identifiable ammonia clouds since the instrumental field-of-view covered some 60° in latitude and 40° in longitude (Baines et al., 2002). The first high-spatial-resolution spectral maps providing positive identification of the upper cloud features of Jupiter were made in the 2.73 μm shoulder of the 3 μm band (hereafter referred to as 3 μm band) by the Near Infrared Imaging Spectrometer (NIMS) on Galileo (Baines et al., 2002), followed by the Cassini

*Corresponding author.
E-mail address: atreya@umich.edu (S.K. Atreya).

0032-0633/$ - see front matter © 2005 Elsevier Ltd. All rights reserved.
doi:10.1016/j.pss.2004.04.002

Composite Infrared Spectrometer (CIRS) at 10 μm (Wong et al., 2004a). These observations confirmed the presence of ammonia clouds, but only in a few localized regions, covering less than 1% of Jupiter's area. In view of the above seemingly contradictory evidence, it is important to ask, what is the composition of the rest of the visible clouds? For decades, researchers (e.g., Tomasko et al., 1984; West et al., 1986, 1989; Baines et al., 2002) have suggested that on Jupiter and Saturn, coating of the upper cloud layers of ammonia ice by photochemically produced haze particles can be a major factor in masking its spectral signature. In this paper, we investigate this possibility, first by comparing the results of our thermochemical model with existing observations, then characterizing two most important haze candidates and the effect of their combination. The two haze candidates are aerosols resulting from the condensation of polycyclic aromatic hydrocarbons (PAHs) in the stratosphere, and the much more abundant hydrazine (N_2H_4) haze produced below. The Galileo and Cassini observations that showed the presence of localized, spectrally identifiable ammonia clouds (SIACs) on Jupiter are summarized in the next section. We note that the ammonia cloud particle effect could be another factor.

2. Galileo NIMS and Cassini CIRS observations of SIAC

Baines et al. (2002) reported the first spectroscopic detection of discrete ammonia ice clouds in the atmosphere of Jupiter. SIACs were found to cover less than 1% of the globe, as measured in the 3 μm absorption band in complete global imagery obtained in September 1996 with the Galileo/NIMS. Rather than coinciding with the major axisymmetric cloud systems, these SIACs were found to be localized in discrete areas, each occupying less than a few degrees of latitude and longitude. The most prominent features were found to be associated with regions of dramatic vertical uplift (Baines et al., 2002). In particular, the spectrally strongest SIACs were found to be associated with the turbulent region to the northwest of the Great Red Spot (GRS), while the majority of the spectrally prominent SIACs were found to lie within a 5°-wide latitudinal band within the North Equatorial Region (NER), associated with a three-dimensional planetary Rossby wave. The remarkable agreement between (1) the observed positions of SIACs relative to 5-μm hot spots, and (2) the theoretical locations of freshly forming ammonia clouds and hot spots predicted by the Rossby wave model of Friedson and Orton (1999) quantitatively reveals that two of the most extreme aerosol structures on Jupiter—the nearly cloudless and volatile poor 5-μm hot spots and the optically thick, ammonia-rich SIACs nearby—are manifestations of a single dynamical mechanism.

Baines et al. (2002) also demonstrated a young age of a few days to a week for the most prominent SIACs. Specifically, for the Rossby wave features in the NER, they found that an age of a few days was consistent with both (1) the lifetime of particles as observationally determined by the wave phase speed and longitudinal cloud width and (2) the sedimentation time for 10 μm radius ammonia particles previously detected by Brooke et al. (1998) in global ISO measurements. A young age for SIACs cloud particles was also indicated for the cloud particles in the major SIACs observed northwest of the GRS. There, Voyager movies indicate that a dramatic flow of turbulent air is produced by the clashing of two opposing zonal jets as they are diverted in their courses by the GRS, which acts essentially as an obstacle in their paths. Specifically, this is where a jet of eastward flowing air to the northwest of the GRS abruptly encounters a southwestward-flowing jet of air which originated as a westward flowing jet to the east of the GRS, but was diverted counterclockwise around it. SIACs were observed repeatedly by NIMS at this location during Galileo's first 4 years in Jupiter orbit. Baines et al. (2002) speculated that due to the three-dimensional interactions of these flows, relatively large amounts of ammonia gas are steadily transported from the sub-cloud troposphere (below the ~600 mb level) to the high troposphere, nearly continuously forming fresh ammonia ice clouds to the northwest of the GRS. A streamline analysis, utilizing the winds deduced by Limaye (1986), showed a lifetime of ~2 days for particles created at the "head" of the feature (where the spectral signature of the ammonia ice is the strongest) as they dissipated downstream. A relatively large particle size for cloud features in the GRS turbulent region is indicated from the high reflectivity observed at 4.05 μm in NIMS imagery (Dyudina et al., 2001). Analysis of this feature by Baines et al. (2003) indicates particle radius of ~2 μm from quantitative modeling of this and other NIMS wavelengths, and more recent analysis shows a better fit for particle radius of ~3.4 μm.

While the sedimentation of large particles may explain the short ammonia particle lifetimes observed in the most dynamic regions of the NER Rossby wave and the GRS turbulent wake regions, nevertheless, planet-wide several factors suggest that non-dynamical processes may also be important in limiting the lifetimes of spectrally identifiable ammonia particles. The small area and nearly circular shapes of SIACs observed across the planet are strong indicators of short particle lifetimes for spectrally identifiable ammonia aerosols. For example, all equatorial SIACs observed extend less than 6° in longitude and 4° in latitude, averaging less than 2.8° in each dimension, in sharp contrast to the dominant

axisymmetric cloud patterns found in various cloudy zones encircling the planet.

In addition to the 3 μm absorption band, ammonia ice has an absorption band at 9.46 μm (1050 cm^{-1}) due to the N–H bend vibrational mode. The 10 μm absorption feature falls in a region of Jupiter's thermal infrared spectrum that is influenced by ammonia gas absorption, collision-induced hydrogen absorption, phosphine absorption, and aerosol scattering and absorption, but subject to constraints on the ammonia ice aerosol size, shape, and vertical distribution, the ice signature can be detected in the data acquired by the Cassini/CIRS during the 2000/2001 encounter with Jupiter. The identification of an ammonia ice feature by Wong et al. (2004a) utilized the low-latitude portion of a global map of Jupiter taken on 31 December 2000 and 01 January 2001, with a spectral resolution of about 3 cm^{-1}. This narrow absorption feature was detected in the continuum between stronger ammonia gas absorption centered at 1054 and 1066 cm^{-1}, in some of the CIRS spectra (Wong et al., 2004a). For example, a spectrum from the 23.5°N region is well matched by the synthetic spectrum including a cloud of ammonia ice particles near 1 μm in size, with a total optical depth of 0.75, while a spectrum from 15°N does not exhibit the ammonia ice feature. The particles detected via this 10-μm ammonia ice feature are smaller than the 2–30 μm ammonia ice particles invoked to fit the Jovian spectra at 3 μm by Brooke et al. (1998) and Baines et al. (2002), and at 10 μm by Marten et al. (1981), Orton et al. (1982), and Shaffer et al. (1986).

The spectral shape of the 10 μm ammonia ice feature is strongly dependent on particle size and shape. Wong et al. (2004a) found a good fit between a CIRS spectrum at 23.5°N, and synthetic spectra including 4:1 prolate spheroid ammonia ice particles with volume-effective radii of 0.79-μm (analogous to a chain of four 0.5-μm spheres). They identify two key conditions for detecting the 10 μm ammonia ice feature: (1) the particle's effective radius must be within a factor of 2 from 1-μm, and (2) the cloud must be present at about the 500-mb level. The ice signature in the 23°N spectrum is well modeled by a cloud with an extended particle-to-gas scale height ratio $H_p/H_g = 1$, with the peak ammonia ice contribution to the opacity coming from around the 500-mb level. These characteristics are more suggestive of an extended haze than of the deeper, more compact cloud ($H_p/H_g = 1/8$) predicted by cloud condensation models (e.g., Weidenschilling and Lewis, 1973; Atreya et al., 1999) and retrieved from observations in the visible (e.g., Banfield et al., 1998) and infrared (e.g., Orton et al., 1982; Marten et al., 1981; Shaffer et al., 1986; Brooke et al., 1998). However, in both the spectrum with the NH_3 ice feature and the spectrum without it, Wong et al. (2004a) require an additional deeper cloud with an essentially gray extinction spectrum, well-modeled by 10-μm NH_3 ice spheres.

3. Jupiter's cloud model

The equilibrium cloud condensation models (ECCM) of Jupiter date back to the pre-Voyager epoch. The first such model was developed by Weidenschilling and Lewis (1973). We use an implementation that has undergone further development as described in Atreya and Romani (1985). The lifting condensation level (LCL) is calculated by comparing the partial pressure (e) and the saturation vapor pressure (e_c) of the condensible volatile. The base of the cloud, LCL, occurs at the altitude where $e = e_c$, i.e. where relative humidity ($q_c = e/e_c$) of 100% is reached. The amount of condensate in the ECCM is determined by the temperature structure at and above the LCL. The release of latent heat of condensation modifies the lapse rate of the atmosphere. We refer the reader to Atreya and Romani (1985) and Atreya et al. (1999) for full details of the current ECCM. Presently no comprehensive model including full treatment of both atmospheric dynamics and microphysics is available. However, this is of little concern to the main goal of this paper—identification, or lack of it—of the visible upper clouds of Jupiter. Although the cloud densities calculated by the ECCM represent upper limits and are much greater than any densities that would actually be expected in the Jovian atmosphere, since atmospheric dynamics would not normally support a continuous wet adiabatic ascent through the entire atmospheric column, and microphysical processes lead to a reduction of the cloud density through precipitation, the ECCM is accurate in predicting LCLs for the condensible volatiles. This is clearly evident from a comparison of the ECCM calculations shown in Fig. 1 and the observation of clouds.

Fig. 1 shows results of ECCM calculations for Jupiter, with 1 × solar and 3 × solar condensible volatile abundances in the left panel, and greatly depleted condensible volatiles in the right panel (Atreya et al., 1999) as the Galileo Probe entered one of the driest places—the Sahara Desert of Jupiter The right panel simulates the LCL of clouds detected by the Galileo probe nephelometer at 1.3 bar, and more tenuous ones at 1.6 and 0.55 bar (Ragent et al., 1998). Although the H_2S, and H_2O mixing ratios in the Probe Entry Site (PES) at pressures less than 9 bar are unknown, their extrapolated values from measured mixing ratios at 9–11 bar (Niemann et al., 1998; Atreya et al., 1999; Atreya et al., 2003), together with the NH_3 profile inferred from the attenuation of Galileo probe radio signal (Fig. 2), are consistent with those required to simulate the PES cloud observations (Fig. 1). This is a strong evidence that the three cloud layers detected in

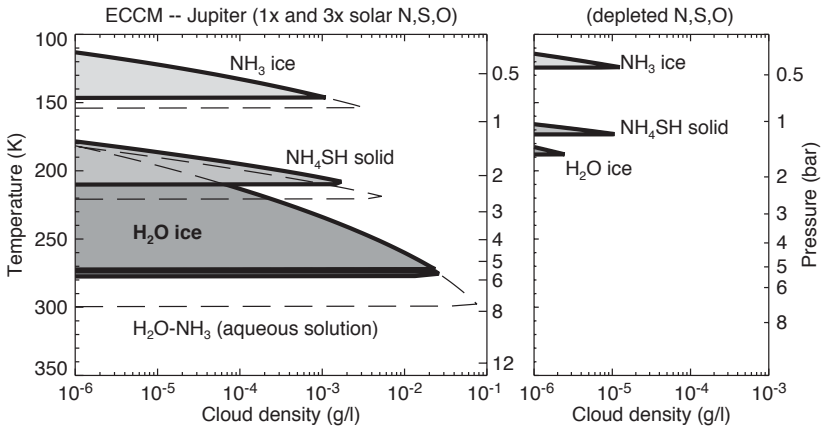

Fig. 1. Left panel: Jovian deep abundances of condensible volatiles were taken at 1 × solar (solid area) and 3 × solar (dashed lines) values (see Table 1), and used to calculate the equilibrium cloud concentrations (in grams per liter). Right panel: as left panel, but with the following depleted condensible volatile abundances relative to solar: H_2O: 0.01%; NH_3: 1%; H_2S: 0.5%. The $p-T$ profile used in the ECCM is from Seiff et al. (1998) for the Galileo probe entry site (right), and modified due to condensation in left panel. (Atreya et al., 1999).

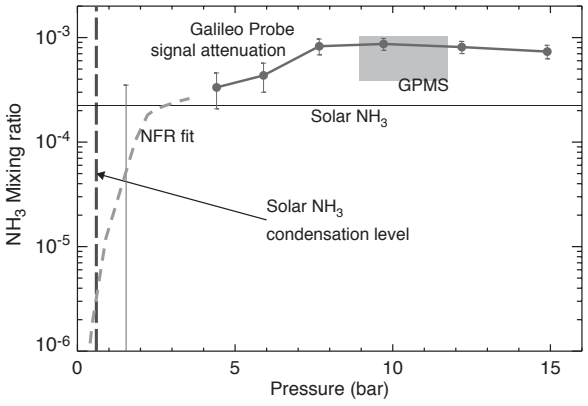

Fig. 2. The variation of the NH_3 to H_2 mixing ratio with pressure based on Galileo Probe Mass Spectrometer (GPMS), attenuation of Galileo probe radio signal (solid line), and the Galileo Probe Net Flux Radiometer (NFR) data (Sromovsky et al., 1998). The base of the NH_3 cloud is predicted by ECCM to be at 720 mb level for solar NH_3/H_2, as shown by the vertical broken line. Note depletion of ammonia in the probe entry site to depths well below expected condensation level. (Atreya et al., 2003).

the probe entry site most likely represent the clouds of NH_3-ice, NH_4SH-ice, and H_2O-ice, with their bases at, respectively, 0.5, 1.3, and 1.6 bar level (Atreya et al., 1999).

Jupiter's N/H elemental ratio is expected to be (3–4) × solar based on measurements of ammonia abundance in the deep well-mixed atmosphere from Galileo probe-to-orbiter signal attenuation (Folkner et al., 1998) and the GPMS measurements (Wong et al., 2004b; Atreya et al., 2003), as in Table 1. The ECCM calculations show that ammonia would condense to ammonia ice at ~500 mb for 0.01 × solar N/H, at 600 mb for 0.5 × solar N/H, at 720 mb for 1 × solar N/H, at 750 mb for 1.2 × solar N/H, at 840 mb for 3 × solar N/H, and at 1000 mb for 4 × solar N/H (see Fig. 1 for some cases). Recently, extensive observations of Jupiter's upper visible clouds at relatively high spatial resolution were done with the Galileo orbiter imaging system at visible and near infrared wavelengths (727, 756, and 889 nm). From an analysis of the low-mid latitude data, Banfield et al. (1998) identified a nearly ubiquitous cloud with its base at 750 ± 200 mb, and cloud optical depth varying between 0 and 20. The pressure range of the observed cloud bases is consistent with the range predicted by the ECCM for 0.01 × solar $\leqslant NH_3 \leqslant$ 4 × solar.

The opacity variation of the cloud observed by Galileo imaging is not surprising since the ammonia mixing ratio varies over the planet, especially from belts to zones (de Pater, 1986), which would result in variation of cloud concentrations and cloud base pressures. Cloud microphysical processes such as precipitation—that can vary planet-wide—would also affect cloud concentrations and hence opacity. The Galileo NIMS near IR observations (Irwin et al., 2001; Irwin and Dyudina, 2002) and Galileo Probe and HST observations (Sromovsky and Fry, 2002) indicate cloud opacity variations in the 1–2 bar region. We believe the variability in the 1–2 bar region is due to an ammonium hydrosulfide cloud predicted by the ECCM (Atreya et al., 1999; Fig. 1). Indeed, as noted earlier, the Galileo probe detected a cloud at 1.34 bar in a dry region of Jupiter where the probe entered. The Sromovsky and Fry (2002) observations are for the north equatorial belt, a dry, downwelling region where ammonia is found to be depleted relative to the zones (Gierasch et al., 1986; de Pater, 1986; West et al., 1992).

The agreement between the ECCM results on the cloud locations of a dry region (Galileo probe) and

Table 1
Elemental abundances

Element	Sun[a]	Jupiter/Sun	Reference
He/H	0.0975	0.807 ± 0.02	von Zahn et al. (1998), Niemann et al. (1998)
Ne/H	1.23×10^{-4}	0.10 ± 0.01	Niemann et al. (1998)
Ar/H	3.62×10^{-6}	2.5 ± 0.5	Mahaffy et al. (2000)
Kr/H	1.61×10^{-9}	2.7 ± 0.5	Mahaffy et al. (2000)
Xe/H	1.68×10^{-10}	2.6 ± 0.5	Mahaffy et al. (2000)
C/H	3.62×10^{-4}	2.9 ± 0.5	Niemann et al. (1998)
		3.27 ± 0.78	Wong et al. (2004b)
N/H	1.12×10^{-4}	3.6 ± 0.5 (hotspot, 8 bar)	Folkner et al. (1998)
		2.96 ± 1.13 (hotspot, 9–12 bar)	Wong et al. (2004b)
O/H	8.51×10^{-4}	0.033 ± 0.015 (hotspot, 12 bar)	Niemann et al. (1998)
		0.028 ± 0.009 (hotspot, 11–17 bar)	Wong et al. (2004b)
		0.29 ± 0.10 (hotspot, 19 bar)	Wong et al. (2004b)
P/H	3.73×10^{-7}	0.804	Kunde et al. (1982)
S/H	1.62×10^{-5}	2.5 ± 0.15 (hotspot, 16 bar)	Niemann et al. (1998)
		2.75 ± 0.66 (>16 bar)	Wong et al. (2004b)

[a]Anders and Grevesse (1989, here after AG89). It is important to note that reanalysis by Holweger (2001) including the effects of non LTE and solar granulation in the solar photospheric abundances has resulted in lower O/H and higher C/H "central" values than those given in the Table (AG89). However, the uncertainties in the Holweger values are large, so that O/H lies between 4.55×10^{-4} and 6.52×10^{-4} with a "central" value of 5.45×10^{-4}, and C/H lies between 3.05×10^{-4} and 5.00×10^{-4} with a "central" value of 3.91×10^{-4}. Using the central values gives an O/C = 1.4. On the other hand, considering the highest O/H and the lowest C/H values from Holweger yields an O/C of 2.14 which is in quite a good agreement with AG89's 2.35 which itself has an uncertainty of approximately $\pm 10\%$. In view of this, our recommendation for the time being is to continue using the AG89 solar elemental abundances as a reference, keeping in mind that the uncertainties in the O and C abundances could be much greater. Similarly, Grevesse and Sauval (1998) advocate somewhat different solar elemental abundances for Ar, Kr, Xe, N and S than AG89, but with overlapping range considering the uncertainties in the two determinations. Again, we have chosen to continue using the AG89 solar elemental abundances as the reference until firmer results are available.

elsewhere (Galileo imaging) is an indirect argument for ammonia ice as the material of Jupiter's upper cloud layer. The robustness of the ECCM is strengthened by the observations of thunderstorms and lightning from the Galileo (Gierasch et al., 2000; Ingersoll et al., 2000) and Cassini (Dyudina et al., 2004) orbiters that are attributed to the presence of water clouds deeper than 4–5 bars. Indeed, the ECCM calculations show that only water clouds can form in this pressure region, as seen in Fig. 1 (Atreya et al., 1999).

From above discussion, it seems likely that ammonia clouds are widespread on Jupiter. However, Galileo/NIMS and Cassini/CIRS observations find spectrally identifiable ammonia clouds only in certain locations, covering just ~1% of Jupiter (Sec. 2). The question arises, why is there no ammonia ice signature in the rest of the visible upper clouds? We discuss the possibility that hydrocarbon particles falling from the stratosphere (Sec. 4) combined with hydrazine haze produced below coat the ammonia cloud particles, thus masking their spectral signature. Baines et al. (2002) suggested also photochemical solid state chemistry ("tanning"), as proposed previously for stratospheric hydrocarbon condensates in Uranus (Pollack et al., 1987) and Neptune (Baines and Smith, 1990). However, Jupiter's clouds lie at pressures several orders of magnitude greater than the Uranian and Neptunian stratospheric condensates, where the ultraviolet flux is severely limited by overlying molecular extinction. Therefore, coating of ammonia particles by other substances, as has been suggested for Saturn (Tomasko et al., 1984), is a more likely mechanism for this ammonia "cover up" (Baines et al., 2002). In both of the tanning and coating processes, clouds begin with relatively bright continua and large ice absorption spectral features. As they age, it is expected that the continua darken slightly and the absorption features are washed out. In the following section, we discuss the nature of hydrocarbon haze that we propose eventually mixes with hydrazine haze near the tropopause, and coats the underlying ammonia clouds.

4. Haze from the stratosphere

On Jupiter, haze particles are formed mainly by condensation of polycyclic aromatic hydrocarbons (PAHs). Other possible haze formation mechanisms include condensation of hydrazine (N_2H_4, Atreya et al., 1977), polyyne polymer ($C_{2n+2}H_2$, $n \geqslant 1$) as on Titan (Yung et al., 1984; Wilson and Atreya, 2003), and HCN polymer (Kuhn et al., 1977; Atreya, 1986), as illustrated in Fig. 3. Any haze from phosphine photochemical products would be insignificant. For the production of PAHs, chemistry begins with the destruction of methane (CH_4) by solar UV photons at $\lambda \leqslant 160$ nm, ultimately

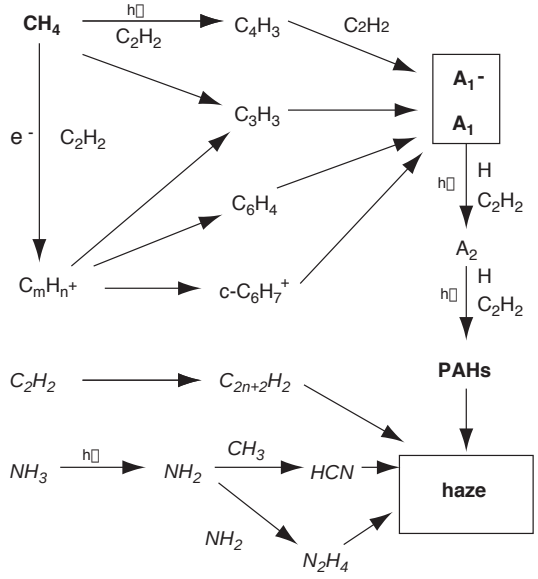

Fig. 3. Illustration of important reaction pathways of haze formation on Jupiter. A_1 is benzene, A_1- is one ring radical, A_2 is naphthalene, and PAHs represents all ring compounds larger than A_2. The pathways beginning with C_2H_2 and NH_3 at the bottom of the figure are minor contributors to haze formation.

leading to the formation of benzene (c-C_6H_6, or A_1) and other complex hydrocarbons (Fig. 3). In the polar auroral regions where energetic particles also break down methane, ion chemistry becomes dominant in the production of benzene and heavy hydrocarbons (Wong et al., 2003, and Fig. 3). In this section, we describe the major benzene production pathways on Jupiter studied using a chemical model (Wong et al., 2001, 2003), first by neutral reactions, and then by ion-related reactions. We then describe the production mechanisms of PAHs and subsequently, haze particles. The results of a microphysical model for haze production (Friedson et al., 2002), summarized below, are found to be in good agreement with available observations. We suggest that the PAH-initiated haze particles are the biggest contributors to the haze that we believe coats the underlying ammonia clouds of Jupiter.

The most important neutral pathway for benzene formation is the recombination of propargyl radicals (C_3H_3), forming either hexatriene (l-C_6H_6) or phenyl radical (c-C_6H_5, or A_1-), which subsequently convert to benzene. The formation of C_3H_3 starts with photolysis of CH_4, followed by addition of H atoms and acetylene (C_2H_2). The maximum production region for this pathway is around 1 mb. This pathway contributes to over 70% of the total benzene production in a mid-latitude neutral photochemical model, as discussed later. Another important neutral pathway is the addition of C_2H_2 to C_4H_3 to form A_1-, contributing 28% to the total benzene production. C_4H_3 is formed by photolysis of C_2H_2 at $\lambda \leqslant 180$ nm, and addition of C_2H_2 and H atoms. The maximum production region for this pathway is around 0.1 mb level.

In the auroral regions, ion chemistry plays a definitive role in hydrocarbon chemistry. A auroral model (Wong et al., 2003) shows that over 97% of benzene is produced through the electron recombination of ring ion c-$C_6H_7^+$, which is formed through successive ion-neutral reactions of ions with C_2H_2 or H_2, producing $C_2H_3^+$, $C_4H_3^+$ and c-$C_6H_5^+$ (Fig. 3). Ion chemistry also promotes production of benzene through neutral reactions by enhancement of neutral hydrocarbon species. For example, ion reactions in the auroral model produce nearly twice as much C_6H_4 as in the non-auroral regions. The cyclization of C_6H_4 forms A_1- and A_1. However, this pathway is still insignificant for producing benzene compared to the others discussed above.

Once benzene is formed, PAHs and other complex hydrocarbons can be formed through successive HACA (H-abstraction, followed by C_2H_2 addition) reactions (see Fig. 1 in Wong et al., 2000). Here we present the results of two chemical models of benzene and PAH formation, one is for non-auroral latitudes and one is for auroral regions. The list of reactions and rate coefficients is included in Wong (2001) and updated in Wong et al. (2003). For the non-auroral latitudes, we consider only neutral chemistry and choose 45° latitude for the purpose of illustration. The column production rates of benzene, naphthalene (A_2, $C_{10}H_8$) and PAHs (all ring compounds larger than A_2) are 2.6×10^8, 4.2×10^9, and 1.5×10^6 molecules cm^{-2} s^{-1}, respectively. The peak production for benzene occurs at 1-mb pressure level, as discussed earlier. The peak production of A_2 occurs at pressure level below 1 mb, and between 1 bar and 1 mb for PAHs. The pre-condensation column abundances of A_1, A_2 and PAHs above 50-mb pressure level are 9.7×10^{14}, 5.3×10^{15}, and 2.3×10^{16} molecules cm^{-2}, respectively. The result for benzene is in good agreement with the ISO observation, which inferred an average benzene column abundance of $9(+4.5, -7.5) \times 10^{14}$ molecules cm^{-2} in the region between 45°N and 45°S (Bezard et al., 2001).

In the second case, ion chemistry is included in an auroral model of latitude 60° (Wong et al., 2003). The auroral stratosphere has a much higher temperature due to particle heating, and the temperature profile is taken from an auroral thermal model of Grodent et al. (2001) to simulate a diffuse aurora with 30.5 ergs cm^{-2} s^{-1} energy flux. The eddy diffusivity profile, $K(z)$, in the auroral regions is assumed to be 15 times greater than that at low latitudes, because the eddy mixing is expected to be much more effective due to the intense energy input (Atreya et al., 1981; Wong et al., 2003). A factor much greater than 15 would result in too fast a transport of species into the interior, and a factor much

less than 15 would result in inefficient transport of ion reaction products away from the regions of peak ion production. The column production rates of A_1, A_2 and PAH are 2.1×10^9, 2.4×10^{10}, and 7.4×10^6 molecules $cm^{-2}\,s^{-1}$, respectively, and the corresponding column abundances are 4.3×10^{15}, 7.3×10^{15}, and 1.1×10^{16} molecules cm^{-2}. Although the production rates of heavy hydrocarbons are 5–10 times greater in the auroral region, when compared to that in mid-latitudes, their abundances are not much greater due to the more efficient eddy mixing in the auroral zone. The peak production of A_1 is at 0.01 mb, the region of the peak particle deposition. The peak production region of A_2 and the PAHs is below the 100 mb level, lower than at mid-latitudes. This is due to the faster transport of heavy species with greater eddy mixing.

Friedson et al. (2002) have developed a one-dimensional, coupled photochemical-aerosol microphysical model to simulate the hydrocarbon chemistry and aerosol processes simultaneously. The basic mechanism is summarized here. To form haze particles, the first step is the homogeneous nucleation of A_4 (pyrene, $C_{16}H_{10}$, a hydrocarbon consisting of four fused hexagonal rings) to form tiny primary particles at higher altitude. This is followed by heterogeneous nucleation of the PAHs, A_3 (phenanthrene, $C_{14}H_{10}$, three-ring compound) and A_2 on the A_4 nuclei at lower altitudes. The particles grow by additional condensation of A_2 and A_3 on the nucleated particles and by coagulation, and eventually sediment out to the troposphere.

The polar microphysical model associated with the auroral chemical model outlined above shows that particles grow to mean radii of ~0.09–1.1 μm, with the larger particles residing at depth, and that the total aerosol loading is $\sim5.5\times10^{-6}\,cm^3\,cm^{-2}$ (Wong et al., 2003). From observations done on the International Ultraviolet Explorer, Tomasko et al. (1986) inferred the total amount of haze particles (expressed in terms of total aerosol volume per unit area) to be $2\times10^{-5}\,cm^3\,cm^{-2}$ in the non-auroral region near 40°N, whereas from Galileo Orbiter and Hubble Space Telescope imaging observations, Rages et al. (1999) derived a value of $\sim3\times10^{-5}\,cm^3\,cm^{-2}$ in the region of 60°N. The predicted aerosol content is somewhat weaker than observations, but probably lies within the model uncertainty which can be resolved only with proper laboratory work. On the other hand, the altitude of the haze top and the mean particle sizes predicted by these simulations are generally consistent with available observations (Tomasko et al., 1986; Rages et al., 1999). For example, the model predicts the haze top of 0.5-μm-size particles at ~1 mb and that most of the particles lie above the 100 mb level, in agreement with observations.

The chemical models above show similar amounts of pre-condensation PAHs in non-auroral regions as in auroral regions, which in turn is expected to lead to similar amounts of haze particles in the two regions of Jupiter. The observations mentioned above (Tomasko et al., 1986; Rages et al., 1999) show similar amounts of total aerosol loading in both polar and non-polar regions, implying that haze particles are ubiquitous in the atmosphere of Jupiter. The model calculations in this section show that PAHs-induced aerosol particles are the main source of stratospheric haze on Jupiter.

5. Discussion and conclusion

As seen above, the principal pathway leading to the formation of haze in the stratosphere of Jupiter begins with the formation of PAHs. In laboratory combustion experiments, PAHs are an important precursor to soot (Richter and Howard, 2000). Although the Jovian environmental conditions are dissimilar to combustion, at least in the polar auroral regions, a large influx of energetic charged particles initially triggers similar chemical processes. The hydrocarbon haze produced in subsequent reactions is believed to be responsible for the UV-dark haze that was first confirmed spectroscopically by Voyager (Pryor and Hord, 1991). Haze is also produced in the non-auroral regions, as discussed in Section 4. The magnitude of non-auroral haze is expected to be somewhat smaller, and its end product composition may be different also. Upon transport of the auroral haze away from the source region, followed by mixing with non-auroral hydrocarbon haze and the much more abundant (white) hydrazine particles below, the haze is likely to take on a grayish appearance in the non-polar regions. In fact, dark haze is detected only in the polar region, although haze is ubiquitous on Jupiter (Sec. 4). Haze particles forming in the stratosphere can take 1–30 years to reach the tropospheric ammonia clouds, if eddy mixing were the only downward transport mechanism. Microphysical processes, including coalescence, coagulation and sedimentation, could reduce the fall times by up to a factor of 100 (Friedson et al., 2002), depending on the altitude and the particle size. Once produced in the stratosphere, hydrocarbon haze particles would fall continuously as soon as steady state is reached. We can estimate the haze particle deposition rate in the following manner.

The observed column abundance of the haze aerosols is $N\sim5\times10^8$ particle cm^{-2} near 40°N (Tomasko et al., 1986). We can assume this value of N to be typical for the planet as a whole in view of the nearly identical aerosol volume (or mass) loading in the polar and non-polar regions (Sec. 4). The mean particle radius is ~0.5 μm near or above the 100-mbar level, deduced from observations (Rages et al., 1999), and would be larger and deeper in the atmosphere due to additional coagulation and condensation (Friedson et al., 2002).

The fall time τ_{fall} for a spherical haze particle of radius 0.5 μm at 100 mb is ~100 times shorter than the eddy diffusion timescale τ_K (Friedson et al., 2002), and the fall times for larger particles are expected to even shorter. At 100 mb, $\tau_K = H^2/K = 10^9$ s ($H \sim 2 \times 10^6$ cm, and $K \sim 3 \times 10^3$ cm^2 s^{-1}, Atreya et al., 1981), and $\tau_{fall} \sim 10^7$ s. This implies a nucleation rate (or production rate) for the haze particles to be $N/\tau_{fall} \sim 50$ cm^{-2} s^{-1}. The column-integrated particle deposition rate is $d \sim VN/\tau_{fall} \sim 3 \times 10^{-11}$ cm s^{-1}, ($V \sim 5 \times 10^{-13}$ cm^3 molecule^{-1}, is the particle volume), or approximately 10 μm/year. If ammonia ice particles are assumed to be spherical rather than flat, the haze layer thickness would be reduced by a factor of eight. However, we suspect that the hydrocarbon haze thickness would still be on the order of a few microns, i.e. comparable to the wavelengths of observations, considering possible shapes of ammonia ice particles.

In fact, the haze layer thickness could be much greater than 10 μm/year. This is because as the hydrocarbon haze from the stratosphere is transported downward, it would mix with the hydrazine ice particles produced in the ammonia photochemistry in the upper troposphere and the lower stratosphere of Jupiter (Strobel, 1973; Atreya et al., 1977). Atreya et al. (1977) calculate a production rate of 6.9×10^{10} hydrazine molecules cm^{-2} s^{-1}, which amounts to as much as 1.3 mg/m^2 per Jovian day of hydrazine condensate (Atreya et al., 1977). Therefore, the hydrazine haze can be orders of magnitude greater than the hydrocarbon haze. Although hydrazine condensate, being white, seems unsuitable as a candidate for masking the spectral signature of the underlying ammonia clouds, its admixture with the hydrocarbon haze is likely to result in a grayish haze material.

Since the ammonia ice particle sedimentation time followed by creation of fresh ammonia particles is also on the order of a year based on current modeling of particle sizes (less than 1 μm; ~0.5 μm in south tropical zone region, Baines et al., 2003), we surmise that a few micron-thick hydrocarbon haze layer would transform the ammonia cloud into a gray cloud, with no distinct spectral signature at 3 or 10 μm wavelengths. Therefore, we suggest that as they fall, the hydrocarbon haze particles coat the upper cloud layer of ammonia ice, and obscure its spectral identification.

Although the haze particles could serve as cloud condensation nuclei (CCN) for the ammonia ice particles, they could adsorb on them as well. However, laboratory work for macroscopic samples shows that small amounts of impurities mixed with water ice, even if the impurities serve as condensation nuclei, can mask the spectral signature of ice (Clark and Lucey, 1984). A similar spectral obscuration of the ammonia-ice cloud is expected only if the contaminant is a significant fraction of the total mass (West et al., 1989; R. Clark, personal communication, 2004), which is a very distinct possibility in view of the large amount of haze produced upon mixing of the hydrocarbon and hydrazine hazes as discussed above. It is also not evident how suitable the haze particles are as CCNs for the ammonia ice particles. Eventually, precipitation would remove the ammonia cloud particles together with the stratospheric haze from the atmosphere.

An important question is whether the NIMS/SIACs lifetime of a few days to a week (Baines et al., 2002, 2003) is due to dynamics or due to their spectral obscuration following the coating by hydrocarbon haze. We estimate that less than 0.1-μm-thick layer of haze would be deposited on the NIMS/SIACs in 1 week. Such a thin layer of haze may not be able to mask their spectral identification, but further laboratory work is needed to confirm this. It is also quite likely that the NIMS/SIACs would dissipate relatively rapidly anyway, considering that they are like convective plumes with large particle size, rising above the main cloud layer. Presently available microphysical and laboratory spectral data are inadequate for calculating the time constants that are essential for distinguishing between the two scenarios. Perhaps a combination of dynamical and haze coating processes is responsible for the relatively short time over which the NIMS/SIACs remain spectrally identifiable. Note also that the SIACs reported by Cassini/CIRS at 10 μm cover data over approximately 1 day (Section. 2), so the lifetime of the CIRS/SIACs is unconstrained.

The cover-up of the ammonia cloud by haze is expected in view of the continuous drizzle of haze particles from the stratosphere, but the ammonia aerosol particle size could also be a factor for the lack of detection of NH_3 ice spectral signature. As discussed in Section 2 and in Wong et al. (2004a), only particles in a narrow range of sizes (about 0.5–2 μm) produce a spectrally distinct absorption feature in the Jovian spectrum near 10 μm. Likewise, calculations presented in Brooke et al. (1998) show that the 3-μm NH_3 ice feature is sharp for 1-μm particles, but broadens for larger particles. Their spatially averaged low-latitude ISO spectrum of Jupiter showed no indication of this sharp feature, a lack that could be interpreted either as evidence for a scarcity of 1-μm particles overall or as evidence that NH_3 cloud particles are coated by precipitating stratospheric haze condensates. Indeed, both Brooke et al. (1998) and Wong et al. (2004a) obtained best fits to ISO and CIRS spectra using atmospheric models that included gray particles in addition to the spectrally distinct NH_3 ice particles. Although the spectral homogeneity of the Wong et al. (2004a) gray cloud component was a shape effect for the large (10 μm) NH_3 particles used, the lack of spectral features in both these particles and the gray particles in the best fit model of Brooke et al. (1998) could

alternately be explained in terms of contamination from precipitating stratospheric haze particles.

In summary, the failure to find widespread signatures of ammonia ice does not necessarily imply that Jupiter's upper cloud layer is not mainly composed of ammonia ice. The hydrocarbon haze produced in the stratosphere, and its combination with hydrazine haze, is expected to play a major role in masking the spectral signature of the upper visible cloud of ammonia. Polyyne polymers, nitrile polymers, as well as meteoritic dust particles, may also contribute to the Jovian haze, but to a much lesser extent. Cloud properties including cloud opacity, cloud physical thickness, cloud top altitude, and the NH_3 aerosol particle size effects can also be a factor in the lack of identification of the upper cloud layer. The SIACs are of course identified as ammonia ice, but the short detection lifetime of NIMS/SIACs may result from dynamical effects or coating by the stratospheric haze or both. Processes similar to Jupiter's must also occur on Saturn, resulting in a spectrally gray ammonia cloud on Saturn also. We encourage laboratory researchers to study optical and microphysical properties including adsorption and CCN characteristics of multi-component systems involving at the very minimum hydrocarbon haze, hydrazine, and the ammonia ice cloud particles.

Acknowledgments

SKA acknowledges support for this research by a grant from NASA's Planetary Atmospheres Program.

References

Anders, E., Grevesse, N., 1989. Abundances of the elements: meteoritic and solar. Geochim. Cosmochim. Acta 53, 197–214.

Atreya, S.K., 1986. Atmospheres and Ionospheres of the Outer Planets and their Satellites. Springer, New York-Berlin, pp. 93–95 and 82–88 (in Chapter 5).

Atreya, S.K., Romani, P.N., 1985. Photochemistry and clouds of Jupiter, Saturn and Uranus. In: Hunt, G.E. (Ed.), Planetary Meteorology. Cambridge University Press, Cambridge, pp. 17–68.

Atreya, S.K., Donahue, T.M., Kuhn, W.R., 1977. The distribution of ammonia and its photochemical products on Jupiter. Icarus 31, 348–355.

Atreya, S.K., Donahue, T.M., Festou, M.C., 1981. Jupiter: structure and composition of the upper atmosphere (theory). Astrophys. J. 247, L43–L47.

Atreya, S.K., Wong, M.H., Owen, T.C., Mahaffy, P.R., Niemann, H.B., de Pater, I., Drossart, P., Encrenaz, T., 1999. A comparison of the atmospheres of Jupiter and Saturn: deep atmospheric composition, cloud structure, vertical mixing, and origin. Planet. Space Sci. 47, 1243–1262.

Atreya, S.K., Mahaffy, P.R., Niemann, H.B., Wong, M.H., Owen, T.C., 2003. Composition and origin of the atmosphere—an update, and implications for the extrasolar giant planets. Planet. Space Sci. 51, 105–112.

Baines, K.H., Smith, W., 1990. The atmospheric structure and dynamical properties of Neptune derived from ground-based and IUE spectrophotometry. Icarus 85, 65–108.

Baines, K.H., Carlson, R.W., Kamp, L.W., 2002. Fresh ammonia ice clouds in Jupiter. I. Spectroscopic identification, spatial distribution, and dynamical implications. Icarus 159, 74–94.

Baines, K.H., Momary, T., Carlson, R.W., Orton, G.S., et al., 2003. The vertical structures and microphysical properties of clouds in Jupiter's Great Red Spot and environs. Division of Planetary Sciences Meeting Abstract, BAAS 35 (4), 994.

Banfield, D., Gierasch, P.J., Bell, M., Ustinov, E., Ingersoll, A.P., Vasavada, A.R., West, R.A., Belton, M.J.S., 1998. Jupiter's cloud structure from Galileo imaging data. Icarus 135, 230–250.

Bezard, B., Drossart, P., Encrenaz, T., 2001. Benzene on the giant planets. Icarus 154, 492–500.

Brooke, T.Y., Knacke, R.F., Encrenaz, Th., Drossart, P., Crisp, D., 1998. Models of the ISO 3-μm reflectance spectrum of Jupiter. Icarus 136, 1–13.

Clark, R.N., Lucey, P.G., 1984. Spectral properties of ice-particulate mixtures and implications for remote sensing I: intimate mixtures. J. Geophys. Res. 89, 6341–6348.

de Pater, I., 1986. Jupiter's zone-belt structure at radio wavelengths. Icarus 68, 344–369.

Dyudina, U.A., Ingersoll, A.P., Danielson, G.E., Baines, K.H., Carlson, R.W., and the Galileo NIMS and SSI Teams, 2001. Interpretation of NIMS and SSI images on the Jovian cloud structure. Icarus 150, 219–233.

Dyudina, U.A., Del Genio, A.D., Ingersoll, A.P., Porco, C., West, R.A., Vasavada, A.R., Barbara, J.M., 2004. Lightning on Jupiter Observed in the H_α line by the Cassini Imaging Science Subsystem. Icarus 172, 24–36.

Folkner, W.M., Woo, R., Nandi, S., 1998. Ammonia abundance in Jupiter's atmosphere derived from attenuation of the Galileo probe's radio signal. J. Geophys. Res. 103, 22847–22856.

Friedson, A.J., Orton, G.S., 1999. A dynamical model of Jupiter's 5-micron hot spots. Bull. Amer. Astron. Assoc 31, 1155–1156.

Friedson, A.J., Wong, A.S., Yung, Y.L., 2002. Models for polar haze formation in Jupiter's stratosphere. Icarus 158, 389–400.

Gierasch, P.J., Conrath, B.J., Magalhaes, J.A., 1986. Zonal mean properties of Jupiter's upper troposphere from Voyager infrared observations. Icarus 67, 456–483.

Gierasch, P.J., Ingersoll, A.P., Banfield, D., Ewald, S.P., Helfenstein, P., Simon-Miller, A., Vasavada, A., Breneman, H.H., Senske, D.A., and the Galileo Imaging Team, 2000. Observation of moist convection in Jupiter's atmosphere. Nature 403, 628–630.

Grevesse, N., Sauval, A.J., 1998. Standard solar composition. Space Sci. Rev. 85, 161–174.

Grodent, D., Waite Jr., J.H., Gerard, J.-C., 2001. A self-consistent model of the Jovian auroral thermal structure. J. Geophys. Res. 106, 12933–12952.

Holweger, H., 2001. Photospheric abundances: problems, updates, implications. In: Wimmer-Schweingruber, R.F. (Ed.), Solar and Galactic Composition. American Institute of Physics, pp. 24–30.

Ingersoll, A.P., Gierasch, P.J., Banfield, D., Vasavada, A.R., and the Galileo Imaging Team, 2000. Moist convection as an energy source for the large-scale motions in Jupiter's atmosphere. Science 403, 630–632.

Irwin, P.G.J., Dyudina, U., 2002. The retrieval of cloud structure maps in the equatorial region of Jupiter using a principal component analysis of Galileo/NIMS data. Icarus 156, 52–63.

Irwin, P.G.J., Weir, A.L., Tayler, F.W., Calcutt, S.B., Carlson, R.W., 2001. The origin of belt/zone contrasts in the atmosphere of Jupiter and their correlation with 5-μm opacity. Icarus 149, 397–415.

Kuhn, W.R., Atreya, S.K., Chang, S., 1977. The distribution of methylamine in the atmosphere of Jupiter. Geophys. Res. Lett. 4, 203–206.

Kunde, V.G., Handel, R.A., Maguire, W., Gautier, D., Baluteau, J.P., Maarten, A., Chedia, A., Husson, N., Scott, N., 1982. The tropospheric gas composition of Jupiter's north equatorial belt (NH_3, PH_3, CH_3D, GeH_4, H_2O) and the Jovian D/H isotopic ratio. Astrophys. J. 263, 443–467.

Limaye, S.S., 1986. Jupiter: new estimates of the mean zonal flow at the cloud level. Icarus 65, 335–352.

Mahaffy, P.R., Niemann, H.B., Alpert, A., Atreya, S.K., Demick, J., Donahue, T.M., Harpold, D.N., Owen, T.C., 2000. Noble gas abundance and isotope ratios in the atmosphere of Jupiter from the Galileo probe mass spectrometer. J. Geophys. Res. 105, 15061–15072.

Marten, A., Rouan, D., Baluteau, J.P., Gautier, D., Conrath, B.J., Hanel, R.A., Kunde, V., Samuelson, R., Chedin, A., Scott, N., 1981. Study of the ammonia ice cloud layer in the equatorial region of Jupiter from the infrared interferometric experiment on Voyager. Icarus 46, 233–248.

Niemann, H.B., Atreya, S.K., Carignan, G.R., Donahue, T.M., Haberman, J.A., Harpold, D.N., Hartle, R.E., Hunten, D.M., Kasprzak, W.T., Mahaffy, P.R., Owen, T.C., Way, S.H., 1998. The composition of the Jovian atmosphere as determined by the Galileo probe mass spectrometer. J. Geophys. Res. 103, 22831–22846.

Orton, G.S., Appleby, J.F., Martonchik, J.V., 1982. The effect of ammonia ice on the outgoing thermal radiance from the atmosphere of Jupiter. Icarus 52, 94–116.

Pollack, J.B., Rages, K., Pope, S.K., Tomasko, M.G., Romani, P.N., Atreya, S.K., 1987. Nature of stratospheric haze on Uranus: evidence for condensed hydrocarbons. J. Geophys. Res. 92, 15037–15065.

Pryor, W., Hord, C.W., 1991. A study of photopolarimeter system UV data on Jupiter, Saturn, Uranus, and Neptune: implications for auroral haze formation. Icarus 91, 161–173.

Ragent, B., Rages, K.A., Knight, T.C.D., Arvin, P., Orton, G.S., 1998. The clouds of Jupiter: results of the Galileo Jupiter mission probe nephelometer experiment. J. Geophys. Res. 103, 22891–22909.

Rages, K., Beebe, R., Senske, D., 1999. Jovian stratospheric hazes: the high phase angle view from Galileo. Icarus 139, 211–226.

Richter, H., Howard, J.B., 2000. Formation of polycyclic aromatic hydrocarbons and their growth to soot—a review of chemical reaction pathways. Prog. Energ. Combust. Sci. 26, 565–608.

Seiff, A., Kirk, D.B., Knight, T.C.D., Young, R.E., Mihalov, J.D., Young, L.A., Milos, F.S., Schubert, G., Blanchard, R.C., Atkinson, D., 1998. Thermal structure of Jupiter's atmosphere near the edge of a 5-μm hot spot in the north equatorial belt. J. Geophys. Res. 103, 22857–22889.

Shaffer, W.A., Samuelson, R.E., Conrath, B.J., 1986. Study of the ammonia ice cloud layer of the North Tropical Zone of Jupiter from the infrared interferometric experiment on Voyager. In: Allison, M., Travis, L.D. (Eds.), The Jovian Atmosphere. NASA Conference Publication 2441, pp. 64–70.

Sromovsky, L.A., Fry, P.M., 2002. Jupiter's cloud structure as constrained by Galileo Probe and HST Observations. Icarus 157, 373–400.

Sromovsky, L.A., Collard, A.D., Fry, P.M., Orton, G.S., Lemmon, M.T., Tomasko, M.G., Freedman, R.S., 1998. Galileo probe measurements of thermal and solar radiation fluxes in the Jovian atmosphere. J. Geophys. Res. 103, 22929–22977.

Strobel, D.F., 1973. The photochemistry of NH_3 in the Jovian atmosphere. J. Atmos. Sci. 30, 1205.

Tomasko, M.G., West, R.A., Orton, G.S., Tejfel, V.G., 1984. Clouds and aerosols in Saturn's atmosphere. In: Gehrels, T., Matthews, M.S. (Eds.), Saturn. University of Arizona Press, pp. 150–194.

Tomasko, M.G., Karkoschka, E., Martinek, S., 1986. Observations of limb darkening of Jupiter at ultraviolet wavelengths and constraints on the properties and distribution of stratospheric aerosols. Icarus 65, 218–243.

von Zahn, U., Hunten, D.M., Lehmacher, G., 1998. Helium in Jupiter's atmosphere: results from the Galileo probe helium interferometer experiment. J. Geophys. Res. 103, 22815–22829.

Weidenschilling, S.J., Lewis, J.S., 1973. Atmospheric and cloud structure of the Jovian planets. Icarus 20, 465–476.

West, R.A., Strobel, D.F., Tomasko, M.G., 1986. Clouds, aerosols, and photochemistry in the Jovian atmosphere. Icarus 65, 161–217.

West, R.A., Orton, G.S., Draine, B.T., Hubbell, E.A., 1989. Infrared absorption features for tetrahedral ammonia ice crystals. Icarus 80, 220–224.

West, R.A., Friedson, A.J., Appleby, J.F., 1992. Jovian large-scale stratospheric circulation. Icarus 100, 245–259.

Wilson, E.H., Atreya, S.K., 2003. Chemical sources of haze formation in Titan's atmosphere. Planet Space Sci. 51, 1017–1033.

Wong, A.S., 2001. Photochemical studies of Jupiter and Titan. Ph.D. Thesis, Caltech.

Wong, A.S., Lee, A.Y.T., Yung, Y.L., Ajello, J.M., 2000. Jupiter: aerosol chemistry in the polar atmosphere. Astrophys. J. 534, L215–l217.

Wong, A.S., Yung, Y.L., Friedson, A.J., 2003. Benzene and haze formation in the polar atmosphere of Jupiter. Geophys. Res. Lett. 30, 1447.

Wong, M.H., Bjoraker, G.L., Smith, M.D., Flasar, F.M., Nixon, C.A., 2004a. Identification of the 10-μm ammonia ice feature on Jupiter. Planet. Space Sci. 52, 385–395.

Wong, M.H., Mahaffy, P.R., Atreya, S.K., Niemann, H.B., Owen, T.C., 2004b. Updated Galileo Probe Mass Spectrometer measurements of carbon, oxygen, nitrogen, and sulfur on Jupiter. Icarus 171, 153–170.

Yung, Y.L., Allen, M., Pinto, J.P., 1984. Photochemistry of the atmosphere of Titan: comparison between model and observations. Astrophys. J. Suppl. 55, 465–506.